10.1098/rsta.2003.1358

THE ROYAL SOCIETY

Chaotic mixing in cross-channel micromixers

By P. Tabeling[1], M. Chabert[1], A. Dodge[1], C. Jullien[2] and F. Okkels[1]

[1]*Microfluidics, MEMS, Nanostructures, ESPCI, 10 rue Vauquelin, 75231 Paris, France* (patrick.tabeling@espci.fr)
[2]*SATIE, ENS-Cachan, Campus de Ker Lann, 35170 Bruz, France*

Published online 12 March 2004

In this article we concentrate on a particular micromixer that exploits chaotic trajectories to achieve mixing. The micromixer we consider here is a cross-channel intersection, in which a main stream is perturbed by an oscillatory flow, driven by an external source. Depending on the amplitude and frequency of the oscillatory flow, one obtains wavy and chaotic regimes, reminiscent of a tendril-whorl mapping. The chaotic states, in which material lines are stretched and folded, favour mixing. A spatiotemporal resonance phenomenon, in which the material-line deformation is transient, is shown. An experiment using soft lithography and integrated valves, in which the resonant states are revealed, is described. From a practical viewpoint, the cross-channel micromixer offers a variety of regimes, which can be exploited to mix fluids or separate particles of different sizes. In the context of microsystems, it can be viewed as a 'smart' elementary system.

Keywords: chaos; micromixing actuation; PDMS; resonance

1. Introduction

Microfluidic systems are too small to shelter turbulence, thus, unlike ordinary-sized systems, mixing in microsystems cannot rely on hydrodynamic fluctuations. Mixing cannot rely on molecular diffusion either, because microsystems are, in many cases, too large for diffusive mixing to be viewed as a fast process. To summarize the situation, one may say that microsystems are often inhospitable to mixing. In a standard lab-on-a-chip device, if nothing is done, it would take hundreds of seconds to carry out sequences of reactions, and this is hardly compatible with the general view that labs-on-a-chip provide fast responses to analytical matters.

These issues were raised in the early 1990s. Since then, more than 20 micromixers have been reported in the literature. This work is reviewed in Reyes *et al.* (2002), Auroux *et al.* (2002) and Tabeling (2003). The first micromixers consisted of dividing channels into small branches, or small nozzles, so as to enhance concentration gradients, and therefore increase diffusive exchanges. This approach has been pushed to an extreme by Knight *et al.* (1998), who obtained mixing times of the order of tens of micrometres. More recent achievements include exploiting Taylor–Aris dispersion

One contribution of 11 to a Theme 'Transport and mixing at the microscale'.

(Scherer & Quake 2000), using viscoelastic properties (Groissman & Steinberg 2001), or producing recirculating flows by means of electrokinetic forces (Ajdari 2000*a*,*b*; Deval *et al*. 2002). We will not review these approaches here. All these micromixers have been shown to 'work', i.e. to mix efficiently, compared with pure diffusion, in some range of experimental conditions; they are usually associated with corteges of constraints and limitations, often difficult to reconcile with integration prospectives, or to adapt to material requirements. This probably explains why, over the past decade, so many microdevices have appeared in the literature. The subject is still open, since we do not have at the moment a universal micromixer which would satisfy all the requirements imposed by microsystem technology and which would fit with all sorts of applications that microfluidic systems are dedicated to. In this respect, the situation is comparable with the one existing in the macroworld.

In the present paper we focus on a particular type of micromixer that attempts to exploit chaotic trajectories. These systems have been proposed in the last five years. They are based on the idea that chaos is remarkably efficient at mixing low-Reynolds-number flows. In essence, the efficiency relies on the fact that, in chaotic regimes, diffusive fluxes across interfaces increase exponentially in time. The idea is not new, since the domain of chaotic mixing or laminar mixing was developed to a remarkable level of sophistication in the 1980s (Ottino 1989). In this respect, it is fair to say that microsystems offer a new field of application for these ideas.

The first design of a chaotic micromixer was published by Evans *et al*. (1997). It consisted of a time-dependent source–sink flow activated thermally, and attempts to adapt a system originally proposed by Aref & Jones (1998). A few years later, Liu *et al*. (2000) (see also Beebe *et al*. 2002) worked at producing a three-dimensional (3D), spiralling chaotic mixer, mimicking the ABC flow configuration, for which it is known that chaotic trajectories exist (Dombre *et al*. 1986). In the same period, Volpert *et al*. (1999) (inspired by the theoretical work of D'Alessandro *et al*. (1999)) and Lee *et al*. (1999, 2001) realized cross-channel micromixers, consisting of one or several channel intersections, operated by using an external oscillatory-flow excitation. This system has recently been analysed in depth, from a dynamical-system perspective, by Niu & Lee (2003). More recently, Stroock *et al*. (2002) exploited 3D vortical flows to produce chaotic regimes along a grooved channel.

The present paper is dedicated to the presentation of the cross-channel micromixer (here called an X-mixer); owing to its simplicity, this mixer may probably be viewed as representative of a broad class of active chaotic micromixers. By investigating chaotic mixing in microsystems one is led to consider unconventional flow configurations, often unexplored because of experimental difficulties to realize them with traditional technologies. This is an interesting situation, prone to uncovering novel phenomena. It so happens that the cross-flow micromixer is the host of a novel phenomenon, a spatiotemporal resonance effect, which, to the best of our knowledge, has not been noticed before. This illustrates the idea that by considering new flow geometries in microsystems, we are likely to expand our knowledge on chaotic systems.

The paper is organized as follows: we first make a presentation of the X-mixer, based on existing work. In this part, we focus on the description of the regimes found in this system, and in particular the chaotic-like regimes, where material lines are subjected to stretching and folding. We further present, in some detail, a spatiotemporal effect called spatiotemporal resonance, which has been revealed recently (Okkels &

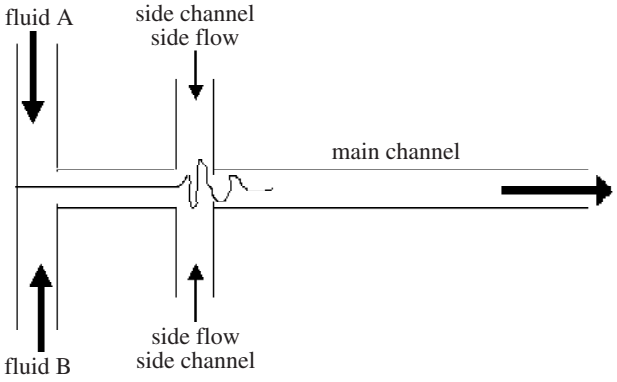

Figure 1. Sketch of the X-mixer. Two miscible fluids (A and B) are conveyed, side by side, towards a cross-channel intersection. At the intersection a time-dependent, additional side flow is driven favouring, under appropriate conditions, mixing between the two fluids.

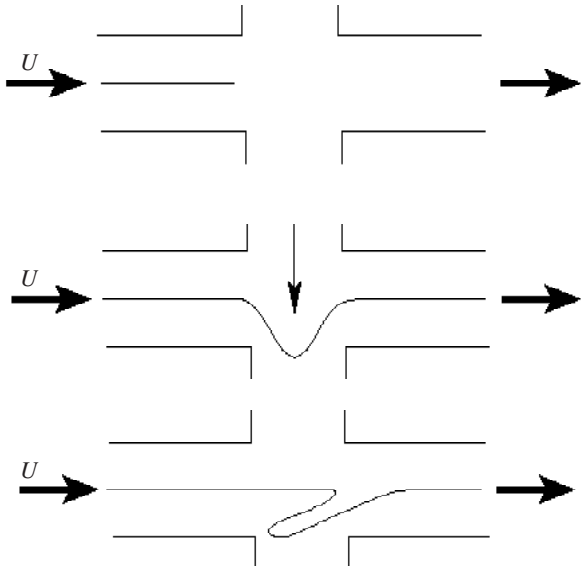

Figure 2. Stretching and folding of an incoming material line as it takes place in the X-mixer.

Tabeling 2004). Finally, we describe an experiment, conducted in our laboratory, which allowed us to observe the resonance phenomenon mentioned above. We conclude by discussing the practical use which can be made of this 'smart' microdevice.

2. Main regimes of the cross-channel micromixer

The geometry of the cross-channel mixer is shown in figure 1. Mixing takes place at the intersection between two channels, one called the main channel and the other the side channel. The main channel has a steady flow and conveys the pair of fluids to be mixed (from left to right in figure 1). The side channels drive a time-dependent flow, with zero net mass flux, superimposed on the main stream. In the intersection, the side flow perturbs the shape of the interface between the two fluids. If the side-flow

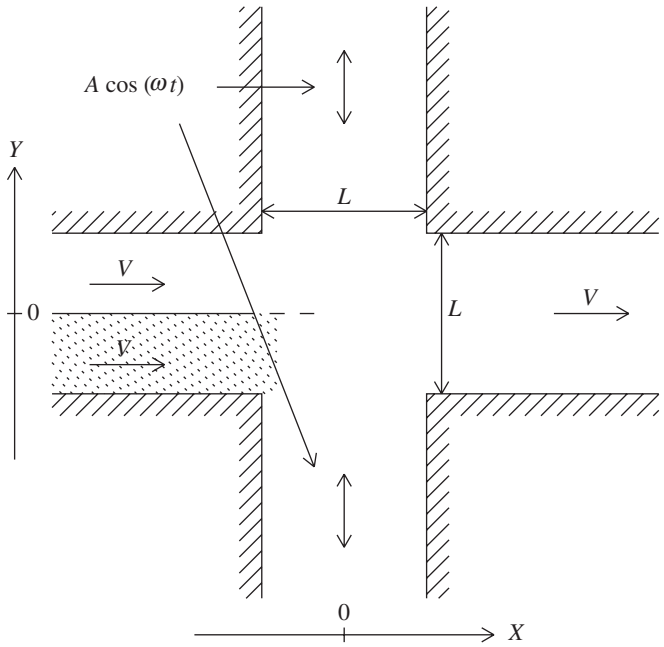

Figure 3. Schematic set-up of the active X-mixer with the characteristic quantities.

amplitude is small, small amplitude waves are generated in the intersection region and further advected downstream. If the side-flow amplitude is large, stretching and folding of the interface can be produced, leading to chaotic states. How can this happen? Figure 2 shows the kinematic mechanism leading to the formation of tendrils and whorls at the interface. Let us consider a material line separating the two fluids upstream. As the material line, advected by the main stream, penetrates into the intersection it gets distorted by the action of the transverse flow and further folded, due to the action of the shearing motion of the main stream. This mechanism is not specific to the X-mixer, it is also involved in a number of phenomena, such as wave-breaking. It is reminiscent of the tendril-whorl map introduced by Khakhar *et al*. (1986).

We performed two-dimensional simulations in order to determine the regimes of the X-mixer. The geometry we considered is shown in figure 3; the magnitude $f(t)$ of the transverse flow velocity $\boldsymbol{V}_{\mathrm{S}}$ changes periodically in time, according to the law $\boldsymbol{V}_{\mathrm{S}} = f(t)\boldsymbol{V}_{\mathrm{T}}$, where $\boldsymbol{V}_{\mathrm{T}}$ is a time-independent vector field, and

$$f(t) = A\cos(\omega t)$$

with amplitude A and angular velocity ω as fixed parameters.

Because of the low Reynolds numbers, the flow equations are linear, and we may superimpose the constant mean-flow $\boldsymbol{V}_{\mathrm{M}}$ with the periodical transverse flow $\boldsymbol{V}_{\mathrm{S}}$ to obtain the total flow. We introduce here the following dimensionless control-parameters:

$$\alpha = \frac{A}{V}, \qquad \Omega = \omega\frac{L}{V}. \tag{2.1}$$

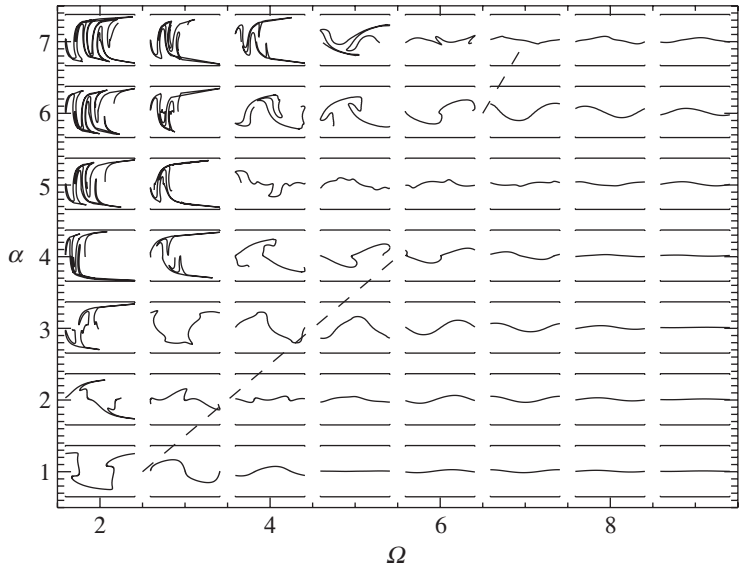

Figure 4. Samples of interface segments positioned at their corresponding control parameter. The dashed line attempts to represent a boundary between folded and non-folded states.

One further obtains the dimensionless governing equations for the X-mixer in the form:

$$\frac{\mathrm{d}X}{\mathrm{d}t} = \boldsymbol{V}_{\mathrm{M}} + g(t) \cdot \boldsymbol{V}_{\mathrm{T}}, \quad g(t) = \alpha \cos(\Omega t). \tag{2.2}$$

In the numerical work, parabolic flow profiles were used in the channels and, to achieve the flow field at the crossing, the full 2D Navier–Stokes equations were solved (by using a finite-difference code in a vorticity–stream function formulation) in the geometry of figure 3. As a result of the numerical integration of (2.2), one obtains the diagram of states displayed in figure 4.

Each elementary picture represents a material line, just after it has crossed the intersection; this segment was initially located upstream in the middle of the main channel, and placed parallel to the main stream. At a small dimensionless amplitude α the material line undergoes weak oscillations, as it passes through the intersection region. This is the 'wavy' regime. As the perturbation amplitude increases, one obtains large-amplitude waves. Chaotic regimes appear at larger perturbation amplitudes, apparently when the wave periodically visits the neighbourhood of the corner of the intersection. When this happens, the material line undergoes one or several foldings and tends to adopt a convoluted periodic pattern downstream, providing some evidence for the presence of an underlying chaotic process, favourable for mixing.

The phase diagram of figure 4 has been observed experimentally, but in far less detail. The corresponding graph, obtained by Y. Lee, C. M. Ho & P. Tabeling (2000, unpublished work), is shown in figure 5.

The experiment was performed in a silicon-glass channel, 400 μm wide and 200 μm deep. The side flow was produced by external pressure reservoirs placed in series with electrovalves, periodically opened and closed in time. In this experiment the amplitude of the forcing was represented by the pressure levels in the side reservoirs.

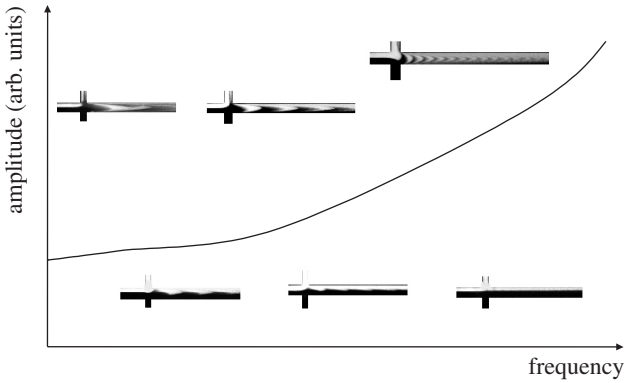

Figure 5. Experimental phase diagram obtained by Lee *et al.* (2001). Horizontal scales are arbitrary, but the order of magnitude of the working frequencies used in the experiment is a few hertz.

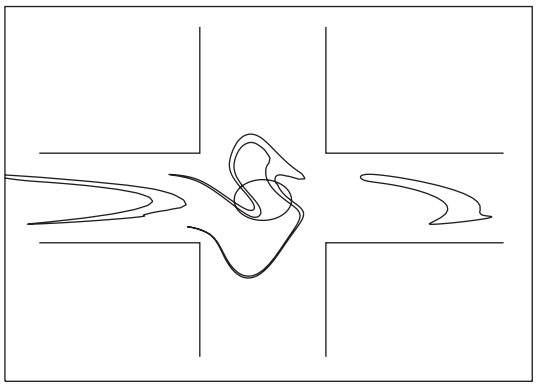

Figure 6. X-mixer with periodic boundary conditions, where snapshots are taken after each full forcing period. The initial round tracer returns strongly deformed to its initial position after three periods, now with a clear horseshoe shape, indicating that the system is truly chaotic.

The working fluids were a solution of sucrose and a solution of sucrose labelled with fluorescein. Detailed analysis of figure 5 indicates that it reproduces clearly a number of states obtained in the simulation. In particular, at small amplitudes of the side-flow perturbation, one obtains wavy-shaped interfaces. As the perturbation amplitude increases, one obtains folded interfaces similar to those of figure 4.

In the mixer considered here, the sequence of folding and stretching only applies a finite number of times. It is possible to increase this number indefinitely by working with periodic boundary conditions in such a way that the flow at the outlet of the intersection is re-injected at the inlet. The result of this approach is shown in figure 6. Here, snapshots are taken after each full forcing period. The initial round tracer returns strongly deformed to its initial position after three periods, now with a clear horseshoe shape, which indicates the presence of a chaotic regime.

Experimentally, this can be achieved by adding several intersections in series, as in Volpert *et al.* (1999). When one has one intersection only, the number of foldings and stretchings is finite, and one may talk of 'chaotic-like behaviour' or, more accurately, of 'finite-time chaos'. This approach, based on finite-time chaos concepts, has been

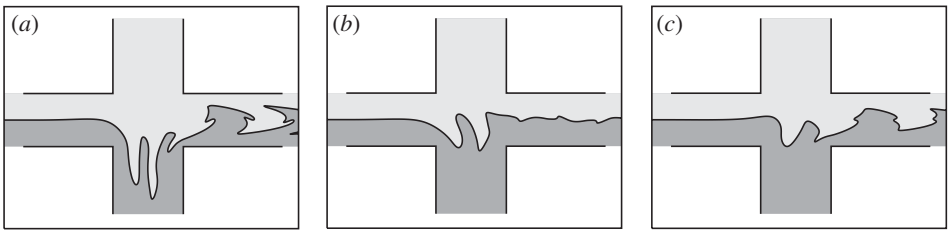

Figure 7. Examples of interface snapshots for different control parameters, showing (*a*) poor mixing $\alpha = 5.85$, $\omega = 5.22$; (*b*) strong mixing $\alpha = 4.85$, $\omega = 5.33$; and (*c*) poor mixing $\alpha = 3.85$, $\omega = 5.33$, and thus strong variations in mixing efficiency in narrow regions of the phase diagram of figure 4.

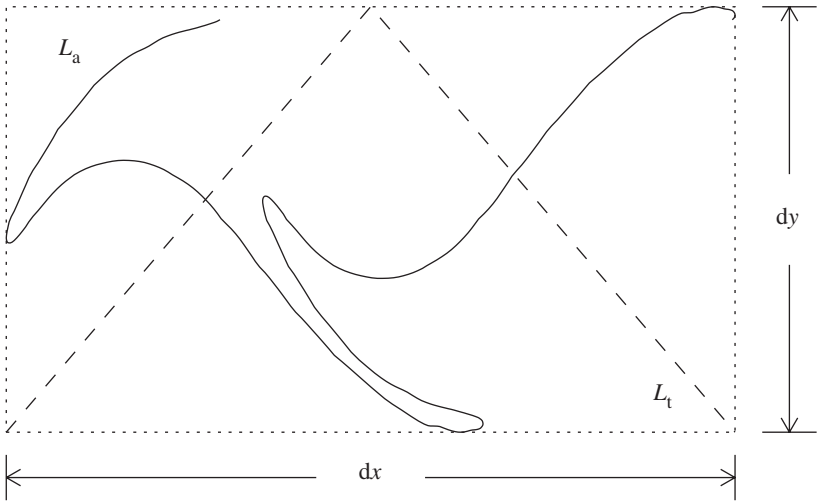

Figure 8. Illustration of how to define the folding quantity F.

developed recently by Niu & Lee (2003). One may note that, in practice, if the fluid diffusion constants lie in an appropriate range, one intersection may be sufficient to obtain well-mixed fluids at the outlet of the X-mixer, as shown in Lee *et al.* (2001).

3. Spatiotemporal resonances

A close inspection of the phase diagram of figure 4 shows that strong variations in folding can occur within a small region of the operating parameters (i.e. α and Ω); this is illustrated in figure 7, where snapshots of the interface in the mixer are shown for different values of the control parameters. One can see a state of poor folding (*b*) inbetween states of better folding (*a*), (*c*). This indicates a more complex dependence on the control parameters. It turns out that bands of poor folding enter into regions of otherwise strong folding, and we will denote these bands as resonances, as justified later in this article.

In order to investigate the phenomenon shown in figure 7, we introduce the following quantity

$$F = \frac{L_a}{L_t} - 1, \quad \text{with } L_t = \sqrt{dx^2 + 4dy^2},$$

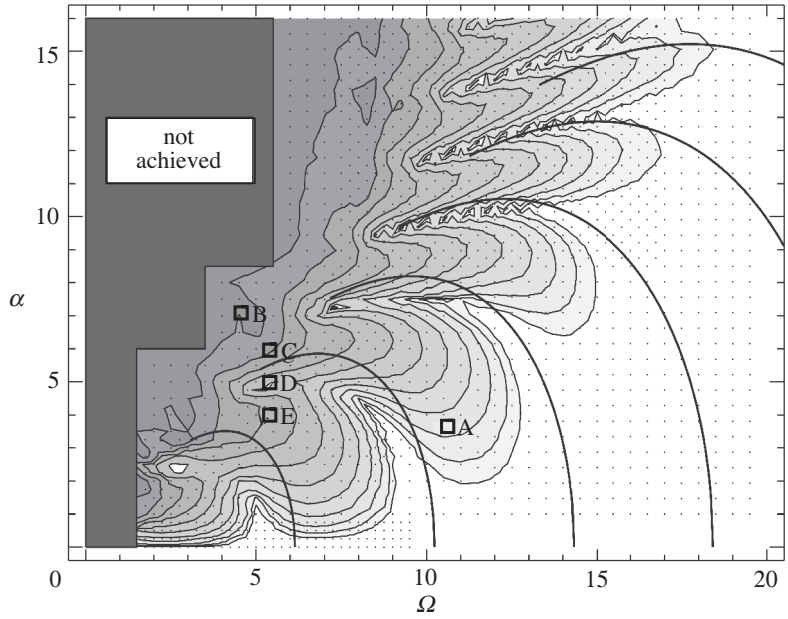

Figure 9. Contour plot of the folding quantity (F) as a function of the control parameters (Ω, α): each measurement of F, points; states shown in figure 7, squares; and theoretical predicted resonances, solid lines.

where L_a is the actual arc length and L_t is a trapezoidal arc length of the same horizontal and vertical dimensions (dx and dy) as of the segment (dx and dy). Figure 8 represents the definitions of the two quantities.

Because of the periodic nature of the forcing, we need only study the interface segment corresponding to one forcing period. Lengths dx and dy are chosen so as to produce a full coverage of the interface at the outlet of the intersection, with boxes of minimal sizes. For $\alpha \to 0$ the interface segment becomes sinusoidally perturbed, making its arc length approach L_t of the corresponding trapezoid. F approaches zero for light perturbations and increases with the complexity of the folding. The folding quantity F has been mapped through a region of the parameter space (Ω, α) and is shown as a contour plot in figure 9 with filled contours increasing in near-logarithmic steps, coloured with darkness proportional to F.

One sees resonances (light) penetrating into regions of good mixing (dark) in such a way that, in the phase diagram of figure 9, well-mixed regions are shaped like dark tongues. The three squares C, D and E in figure 9 correspond, respectively, to the three interfaces shown in figure 7*a–c*, which confirms the poor mixing seen in part (*b*) as it is positioned on a resonance. The resonances arise when the perturbation of a point on the interface during the first half of the cross-section is completely reversed during the last half, resulting in a vanishing net perturbation.

In our simple flow geometry, resonances can be further discussed by comparing the period of the forcing $T_P = 2\pi/\Omega$ and the advection time through the active-mixing region of a point on the interface T_A, located, initially, at the centre of the upstream channel close to the intersection region. To be in a resonant tongue, one must have

the following relation between these two characteristic time-scales:

$$T_{\mathrm{A}} = C_n T_{\mathrm{P}}, \quad \text{where } C_n \approx n + \tfrac{1}{2}, \tag{3.1}$$

where n is an integer. Equation (3.1) justifies the notion of 'resonances', as it relates two characteristic time-scales of the mixer. The resonance relation has been checked theoretically by first deriving an approximative analytic expression of T_{A} as a function of α and Ω, and then using the resonance relation between T_{A} and T_{P} to estimate the position of the resonance tongues in the (α,Ω)-plane. This has been done and the estimated resonance tongues are shown in figure 9 (solid lines), giving a good qualitative and quantitative agreement with the numerical results.

When the mixer is tuned at a resonance, the interface becomes symmetric (antisymmetric) along the transverse direction, as the phase of the forcing is $0, \pi$ ($\pi/2$, $3\pi/2$). This is due to an interplay between the temporal symmetries of the forcing and the spatial symmetries of the flow geometry, and this gives a clear indication of resonant states, which will be used later to validate the theory experimentally. It also underlines the spatiotemporal nature of the resonances.

4. Experimental observations on the X-mixer

(*a*) *Introduction*

We now come to the experimental study of the X-mixer. As mentioned in § 1, several experimental studies have been carried out to investigate the properties of the cross-channel mixer. In particular, it has been shown that the micromixer 'works', i.e. it has an ability to mix miscible fluids in some range of experimental conditions (Y. Lee, C. M. Ho & P. Tabeling (2000, unpublished work); Lee *et al*. 2001; Volpert *et al*. 1999). The unpublished research of Y. Lee, C. M. Ho & P. Tabeling (2000), which led to the production of figure 5, provided evidence concerning the presence of stretching and folding at the interface. We focus here on a new device, for which the control has been improved, and which provided qualitative observations of the aforementioned resonance states.

(*b*) *Experimental system*

The layout of the device with its operation mode is illustrated in figure 10. It consists of a main channel, where two streams of glycerol flow side by side, one flow being marked with fluorescein and the other not. A series of 10 integrated poly(dimethylsiloxane) (PDMS) valves are laid out in a comb-shaped fashion onto two channel branches perpendicular to the main flow. These valves are made by using multi-layer technology (called MSL, see Unger *et al*. (2000)). They include actuation channels filled with water; these channels compress a membrane, closing or opening a segment of a microfluidic channel, depending on the pressure applied to them. A sketch of such a valve is shown in figure 11.

As the comb-disposed valves close on one branch, they create a displacement of fluid at the channel intersection located at the centre of the device. The displacement amplitude is proportional to the surface of the actuation valves and the pressure applied to the actuation channels. Releasing the pressure applied to one comb and applying pressure on the other comb creates a flow in the opposite direction. Therefore, it is possible to create an oscillating flow with a certain frequency and amplitude

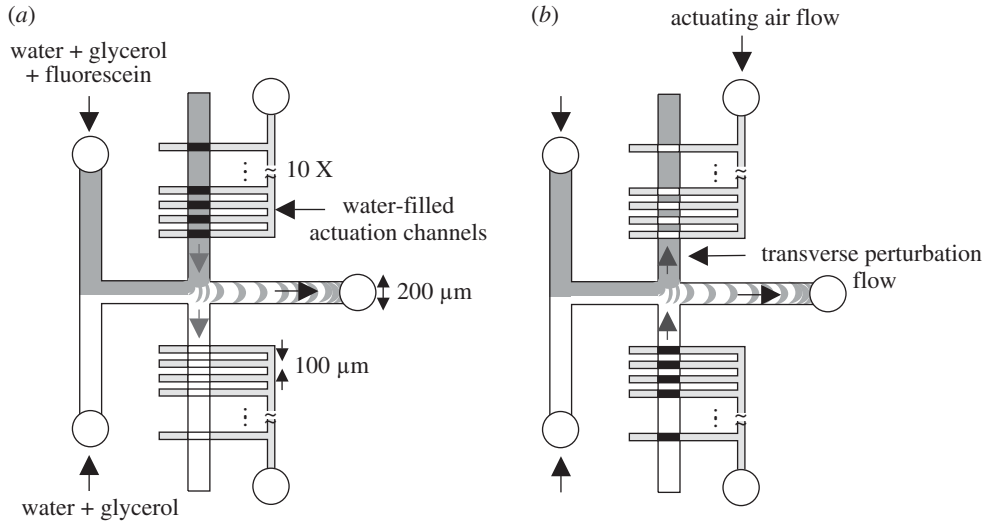

Figure 10. Layout of the experimental system used in the article with the operation mode: (*a*) upper valves closed, lower ones open, producing a side flow oriented downwards; (*b*) opposite movement, producing an upwards side flow.

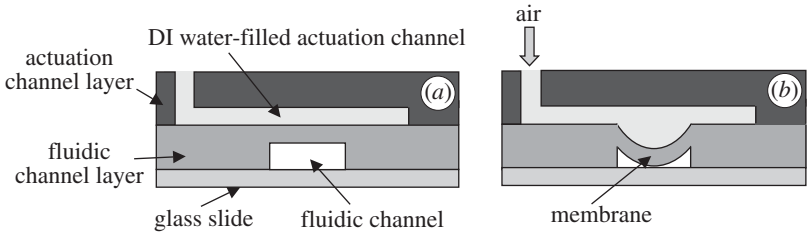

Figure 11. PDMS valve actuation: (*a*) working channel open; (*b*) working channel closed.

at the cross-channel intersection. The frequency will depend on the speed at which the combs are switched. The main flow is therefore perturbed by a well-controlled transverse, oscillating periodic flow created at the cross-channel intersection. Control of the perturbation of both amplitude and frequency is excellent with this method.

Concerning the details of the microfabrication, the experimental procedure was as follows: SU8 2015 photoresist (Chimie Tech, Antony, France) was spun at 1000 RPM on a 2 mm thick polished silicon wafer to obtain SU8 mould-feature heights of 26 µm. Fluidic channels were fabricated by spinning 1:20 Sylgard PDMS (Corning, France) onto an SU8 mould at 1200 RPM and baking for 20 min. Actuation channels were fabricated by depositing a 5 mm thick layer of 1:10 PDMS onto an SU8 mould and polymerizing for 40 min at 75 °C. Holes were then punched into the actuation channel layer for the creation of access channels to it. The two layers were aligned, put in contact with one another and heated at 75 °C for 4 h to finish polymerization. Holes were then punched through the two-layer device creating access to the fluidic channels. A Menzel–Gläser microscope slide (Fisher Bioblock, Illkirch, France) was cleaned with analysis-grade acetone and isopropanol (SdS, Vitry, France) and dried with nitrogen gas (Air Liquide, Nanterre, France). The PDMS structure and the glass slide were exposed to a plasma treatment for 2 min in a Harrick plasma

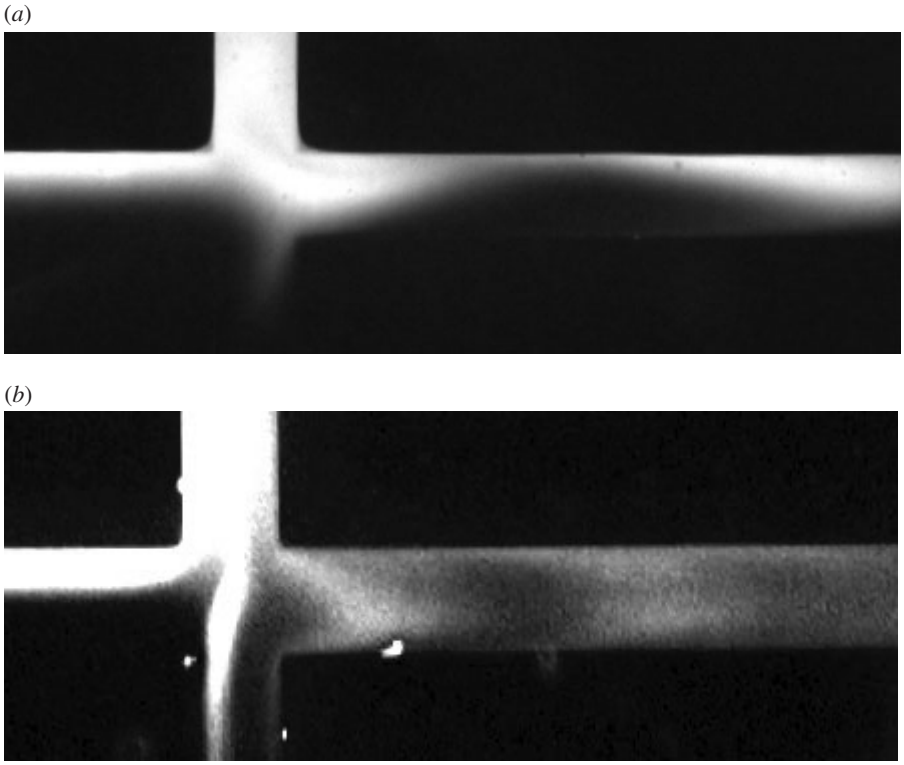

Figure 12. (*a*) Amplitude, 0.5 bars; frequency, 1 Hz. (*b*) Amplitude, 1 bar; frequency, 4 Hz.

cleaner/sterilizer (Harrick, USA) before immediately being brought together to create a permanent bond between the polymer and the glass, thus sealing the fluidic channels.

A homemade electronic circuit driving two LEE valves (LEE, USA) controls the arrival of an in-house network-of-compressed-air line, which pushes DI water located in the actuation channels. PEEKTM tubing (outer diameter 800 μm; inner diameter 200 μm) and fittings (Upchurch, Paris, France) were used to connect the device to the LEE valves. A KD scientific syringe pump (Fisher, France) connected to the device via PEEK tubing was used to bring the different reagents into the fluidic channels at a flow rate of 0.5 μl min^{-1}. A TG1010 function generator (Thurlby Thandar Instruments, Huntingdon, UK) controls the frequency at which the LEE valves are switched, thereby setting the lateral-perturbation frequency. A Cohu charge-coupled device camera (SAIS, St Remy les Chevreuse, France) mounted onto a Leica Binocular MZFL III using a GPFII optical filtering set (Leica Microsystems, Rueil Malmaison, France) was used to take images of the fluorescent patterns created in the microfluidic channels.

(*c*) *Results*

Figure 12 shows several states of flow, consistent with previous experimental studies. At small valve-deformation amplitudes a wavy regime is observed, while at larger deformation amplitudes folded states are obtained. As shown in figure 12, the flow at

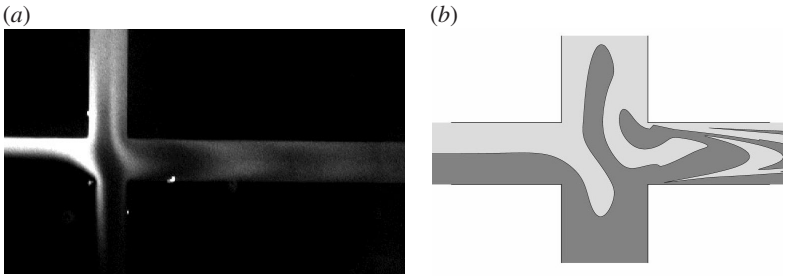

Figure 13. Pattern obtained by (*a*) experimental and (*b*) numerical simulations, showing qualitative agreement.

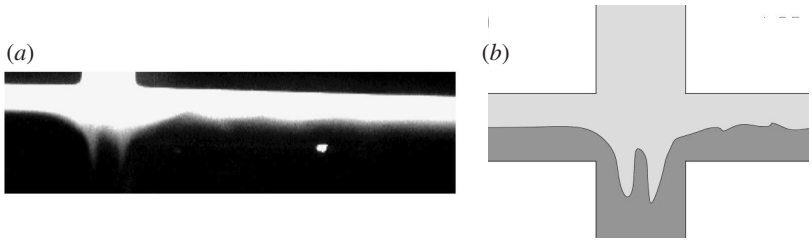

Figure 14. Resonance observed in the experiment. (*a*) experiment, (*b*) numerical simulation.

the intersection folds and reorients fluorescein patches. As the fluorescein blob reaches the outlet of the intersection, the streamwise concentration gradients tend to vanish under the action of Taylor–Aris dispersion. This dispersion process, absent from the 2D simulation, is an additional effect, which complicates the analysis; nonetheless, from the viewpoint of mixing, it contributes to the formation of homogeneous mixtures at the outlet of the mixer unit.

Apart from Taylor dispersion effects, the experiment agrees well with the 2D simulation. This is shown in figure 13, which compares two chaotic-like states, one produced experimentally and the other obtained numerically, using the 2D simulation described previously.

One sees that the numerical simulation agrees well with the experimental simulation; this provides support for a 2D approach to the problem.

The experimental system we describe here permits the observation of resonant states in conditions consistent with those expected theoretically. The observation of an even resonance state is shown in figure 14.

In the case we consider here, the frequency is held at 15 Hz and the imposed flow is $0.5\,\mu\mathrm{l\,min}^{-1}$. The interface is strongly distorted in the intersection and leaves it almost as flat as it enters. Nonetheless, the interface is thicker, showing that diffusion has been enhanced, as a result of the substantial increase of the interface area, in the intersection. Figure 14 indicates that numerical and experimental simulations agree well, at a qualitative level.

(*d*) *Using resonance states to sort particles of different sizes*

The resonant regime may have interesting implications for particle sorting or particle extraction. This aspect is shown in figure 15. The Stokes–Einstein law stipulates that the diffusion coefficient of a particle is inversely proportional to its radius. This

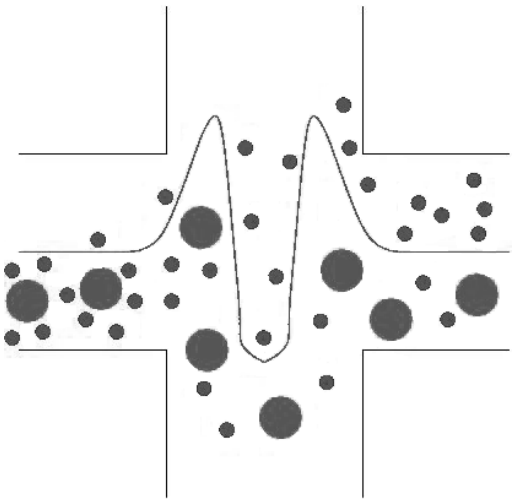

Figure 15. Filtering of particles of different sizes in the resonant regimes: larger particles stay in the lower part of the main channel, while smaller ones cross the interface; this is due to the fact that, in resonant regimes, the exchange area between the lower and upper parts of the flow is momentarily increased in the channel intersection.

implies that two populations of particles, with different radii, located on the same side of an interface separating two miscible fluids, will undergo a demixing process: the smaller particles will diffuse more easily across the interface than the larger ones. Resonance regimes should considerably enhance the separation rate by increasing, temporarily, the interface between the two fluids. This effect is shown in figure 15.

In figure 15, two populations of particles are injected into the lower fluid layer. One expects an efficient demixing process to take place, owing to the fact that the interface area has considerably increased during the time it spends in the intersection. This process is made possible by using resonant states.

5. Conclusion

The cross-channel micromixer offers the opportunity to exploit chaotic trajectories in order to enhance mixing. We also revealed the existence of a spatiotemporal resonance phenomenon in which material lines are elongated and folded as they penetrate in the intersection but come back to their initial shape as they leave it.

One may note that in the resonance regimes the action of the X-mixer achieves, in a controlled way, reversible stretching and folding of material lines. It is not the first time that reversible distortion of material lines is obtained experimentally. The most famous example of reversible stretching is the experiment made by G. I. Taylor decades ago demonstrating the reversibility of Stokes equations. In his textbook, Ottino (1989) shows well-controlled experiments using highly viscous fluids in which a reversible sequence of stretchings and foldings occurs. One advantage of working with miniaturized systems is the possibility of using low-viscosity fluids (such as aqueous solutions) with substantially large stretching rates, while keeping the Reynolds number small. Also, miniaturizing the system offers the possibility to easily increase the complexity of the channel geometry, while maintaining the flow control at an excellent level. The X-mixer illustrates these advantages well.

To summarize, it has been shown in this article that, depending on the experimental parameters fed to the device, the X-mixer can display a number of different regimes, thus offering a versatile unit which can either mix or sort particles. It may thus be viewed as a 'smart' elementary system. At the moment, the X-mixer is one of the rare chaotic-like mixers for which some documentation exists. Nonetheless, although a number of numerical and experimental results are available (see Lee *et al*. 2001; Niu & Lee 2003; Okkels & Tabeling 2004; Volpert *et al*. 1999), it would probably be worth expanding the analysis of this system—in particular to extract quantitative information on the characteristics of chaotic or chaotic-like regimes. Efforts are currently being aimed in this direction, at numerical and theoretical levels (Niu & Lee 2003) and, in our group, at an experimental level.

The authors thank Centre National de la Recherche Scientifique, Ecole Supérieure de Physique et Chimie de Paris, and the EEC (under grant HPRN-CT-2002-00300) for supporting this research. The authors have also benefited from instructive discussions with Y. K. Lee, T. Tel and H. Aref.

References

Ajdari, A. 2000*a* *Phys. Rev.* E **53**, 4996.

Ajdari, A. 2000*b* *Phys. Rev.* E **61**, 45.

Aref, H. & Jones, S. 1998 *Phys. Fluids* **1**, 470.

Auroux, P. A., Iossifids, D., Reyes, D. & Manz, A. 2002 *Analyt. Chem.* **74**, 2637.

Beebe, D., Mensing, G. & Walker, G. 2002 *A. Rev. Biomed. Engng* **4**, 261.

D'Alessandro, D., Dahleh, M. & Mezic, I. 1999 *IEEE Trans. Automatic Control* **44**, 1852.

Deval, J., Tabeling, P. & Ho, C. M. 2002 In *Proc. MEMS 2002, Las Vegas, NV, USA*.

Dombre, T., Frisch, U., Greene, J. M., Henon, M., Mehr, A. & Soward, A. M. 1986 *J. Fluid Mech.* **167**, 353.

Evans, D., Liepmann, D. & Pisano, A. P. 1997 In *Proc. MEMS 1997, Nagoya, Japan*, p. 96.

Groissman, A. & Steinberg, V. 2001 *Nature* **410**, 905.

Khakhar, D., Rising, H. & Ottino, J. 1986 *J. Fluid Mech.* **172**, 419.

Knight, J., Vishwanath, A., Brody, J. & Austin, R. 1998 *Phys. Rev. Lett.* **80**, 3866.

Lee, Y. K., Shih, C., Tabeling, P. & Ho, C. M. 1999 Characterization of mixing processes in a microchannel flow. In *Proc. 52nd Annual Meeting of APS, November 1999, New Orleans, LA*.

Lee, Y. K., Deval, J., Tabeling, P. & Ho, C. M. 2001 In *Proc MEMS 2001, Interlaken*, p. 483.

Liu, R., Stremler, M., Sharp, K., Olsen, M., Santiago, J., Adrian, R., Aref, H. & Beebe, D. 2000 *J. Microelectromech. Syst.* **9**, 190.

Niu, X. & Lee, Y. K. 2003 *J. Micromech. Microengng* **13**, 452.

Okkels, F. & Tabeling, P. 2004 *Phys. Rev. Lett.* **92**, 38301.

Ottino, J. M. 1989 *The kinematics of mixing, stretching, chaos and transport*. Cambridge University Press.

Reyes, D., Iossifidis, D., Auroux, P.-A. & Manz, A. 2002 *Analyt. Chem.* **74**, 2623.

Scherer, A. & Quake, S. 2000 *Science* **290**, 1536.

Stroock, A., Ajdari, A., Dertinger, S., Mezic, I., Stone, H. & Whitesides, G. 2002 *Science* **295**, 647–651.

Tabeling, P. 2003 *Une introduction à la microfluidique*. Collection Echelles. Paris: Editions Belin.

Unger, M., Chou, H., Thorsen, T., Scherer, A. & Quake, S. 2000 *Science* **288**, 113.

Volpert, M., Mezic, I., Meinhart, C. & Dahleh, M. 1999 *Proc. ASME Mechanical Engineering Int. Congr. and Exposition, Nashville, TN*, p. 483.